Detection of small inclusions by elastography

Jérôme Fehrenbach[1], **Mohamed Masmoudi**[1], **Rémi Souchon**[2], **and Philippe Trompette**[2]

[1] Laboratoire MIP, Université Paul Sabatier, 31062 TOULOUSE CEDEX 09, France
[2] INSERM U556, 151 Cours Albert Thomas, 69424 LYON CEDEX 03, France

E-mail: `fehren@mip.ups-tlse.fr`

Abstract.

The problem of parameter identification for elastostatics equilibrium equations in two dimensional inhomogeneous domains is considered. Elastic properties of a linear isotropic material depend on two parameters: Young's modulus E and Poisson coefficient ν, and our objective is to determine the values and the spatial distribution of E in a plane domain Ω, where ν is assumed to be constant. It is assumed that the input data are directional displacements in Ω under a small quasistatic compression, this is consistent with an existing imaging modality called elastography. We prove that this problem involves a compact operator.

A method is proposed here to identify the spatial distribution of E up to a multiplicative factor. It is based on an implementation of Gauss-Newton method that is obtained without the calculation of the Jacobian matrix. It is performed by the use of conjugate gradient, through a combination of reverse (adjoint) and forward (direct) differentiation, that makes sense in the case of compact operators. Our method is validated both with numerical and experimental results.

02.30.Jr, 02.30.Zz, 62.20.Dc, 46.15-x, 46.25-y
2000 MSC classification numbers: 65N21, 74B05, 74G75, 74L15, 74S30

Submitted to: *Inverse Problems*

1. Introduction

Elastic parameters identification is a challenging issue in the medical imaging area. Prostate and breast tumors exhibit a Young's modulus much higher than the surrounding normal tissues. Their detection by clinical palpation requires that the tumor is big or near enough from the surface. Ultrasonic elastography is a displacement imaging technique in soft biological tissues undergoing a small quasi-static or time-dependent compression [1, 2], the image of displacement is called an elastogram. We address in this paper static elastography, where numerous works have already been published, and our goal is to obtain an image of the relative Young's modulus from an elastogram. From the mathematical point of view, given the displacement in the whole domain (or one component of the displacement, along the direction of compression) under a small

quasi-static deformation of a linear isotropic medium, the Young's modulus distribution has to be estimated, up to a multiplicative factor.

Parameter identification problems are often ill-posed and are usually treated as optimization problems [3]. Unfortunately, short term approaches like the steepest descent method are not suitable for elastography in the presence of noise since they are likely to be trapped in a local minimum, see figures 3(c)-3(d). It is also the case of conjugate gradient methods (Fletcher-Reeves and Polak-Ribiere) and BFGS [4], since they behave like the steepest descent method at the first iteration.

We make use here of Gauss-Newton's least squares optimization method [4], it is an approximate second order method and provides information from the model through the Jacobian and its transpose. We prove that each step requires the resolution of an equation involving the inversion of a compact operator. The problem is thus ill-posed, but on the numerical point of view it can easily be solved for, at least approximately, when a regularization term is added [5]. As a matter of fact, a compact operator can be reasonably approximated by a finite sum of a (small) number of rank one operators. Additionally this approximation provides a regularization of the equation. This implies that Krylov subspaces methods, like the conjugate gradient algorithm (CG) in the symmetric positive case, are suitable for inverting compact operators. Indeed, CG gives, after m steps, the (oblique) projection of the solution onto a Krylov space $\mathcal{K}_m$. Since the eigenvalues tend rapidly towards zero, this Krylov space provides a good approximation of the eigenvectors associated to the largest eigenvalues of DF^TDF. The solution will then be approximated after a few iterations of CG [3].

A Gauss-Newton algorithm was applied to elastography in [6, 7, 8], where the Jacobian matrix is entirely computed. Since this method requires high computational resources, it can be used only on coarse meshes, and therefore can detect only large inclusions. An adjoint method [9] has been used in [10] and [11] to compute the gradient as a descent direction in optimization algorithms: a large number of iterations is required to obtain an acceptable image of a large inclusion.

It has been pointed out in [11] that Gauss-Newton method requires too much computational resources. This is true if a naive version of Gauss-Newton algorithm is used, where the whole Jacobian matrix is computed using the adjoint method: one elasticity problem is solved for each column of the Jacobian. On the other hand, the method exposed here does not require the computation of the Jacobian, it is implemented using both forward and reverse modes of algorithmic differentiation [12]. It requires little memory and few computations (at each iteration of conjugate gradient, one direct and one adjoint problem are solved).

This paper is organized as follows: the direct problem in static elastography is described (section 2). The method for solving this compact inverse problem is explained (section 3). In section 4, numerical results are presented and show that our method is efficient, at least at low levels of noise. In section 5, experimental results are presented. The proof of proposition 1 (compactness of the operator involved in elastography) is given in appendix A and the algorithms we use are presented in appendix B.

2. A direct elastostatics problem

We describe in this section the parameter-to-state map involved in elastostatics (under known boundary conditions) and prove that its differential is compact.

Let Ω be a plane bounded Lipschitz domain, and $\partial\Omega = \Gamma_N \cup \Gamma_D$ be a partition of its boundary where Γ_D has positive Lebesgue measure and $\overline{\Gamma_N}$ and $\overline{\Gamma_D}$ are disjoint. We consider an elastostatics problem in Ω with Neumann boundary conditions $g \in H^{-1/2}(\Gamma_N)$ on Γ_N and homogeneous Dirichlet conditions on Γ_D. Let $(\lambda, \mu) \in L^\infty(\Omega) \times L^\infty(\Omega)$. The Hooke tensor $C^{\lambda,\mu}$ is defined by

$$C^{\lambda,\mu}_{ijkh}(x) = \lambda(x)\delta_{ij}\delta_{kh} + \mu(x)(\delta_{ik}\delta_{jh} + \delta_{ih}\delta_{jk}). \tag{1}$$

We say that the Hooke tensor $C^{\lambda,\mu}$ satisfies uniform coercivity, or that the parameter (λ, μ) satisfies uniform coercivity, if there exists a positive constant c such that for all $x \in \Omega$ and all symmetric matrix (ϵ_{ij}),

$$\sum_{ijkh} C^{\lambda,\mu}_{ijkh}(x)\epsilon_{ij}\epsilon_{kh} \geq c \sum_{ij} \epsilon_{ij}\epsilon_{ij}. \tag{2}$$

The set of parameters (λ, μ) that satisfy uniform coercivity is an open set of $L^\infty(\Omega) \times L^\infty(\Omega)$. Let $\sigma_{\lambda,\mu}(u) = C^{\lambda,\mu}.\epsilon(u)$, where $\epsilon(u)$ is the linearized strain tensor. The weak form of the elastostatics problem described above is: find $u \in \mathcal{V}$ such that

$$\forall v \in \mathcal{V}, \qquad a_{\lambda,\mu}(u, v) = \ell(v), \tag{3}$$

where

$$a_{\lambda,\mu}(u, v) = \int_\Omega \sigma_{\lambda,\mu}(u) : \epsilon(v)\, dx, \qquad \ell(v) = \int_{\Gamma_N} g.v\, dl, \tag{4}$$

and $\mathcal{V} = \{u \in H^1(\Omega)^2 \mid u|_{\Gamma_D} = 0\}$. If (λ, μ) satisfies uniform coercivity, it is a classical result [13] that the problem (3) has a unique solution $u_{\lambda,\mu}$.

Proposition 1 *The parameter-to-state map*

$$\begin{array}{rccc} R: & L^\infty(\Omega) \times L^\infty(\Omega) & \longrightarrow & H^1(\Omega)^2 \\ & (\lambda, \mu) & \longmapsto & u_{\lambda,\mu}, \end{array}$$

with $u_{\lambda,\mu}$ solution of (3), is differentiable on the open set where the uniform coercivity is satisfied. Hence the map

$$\begin{array}{rccc} \overline{R}: & L^\infty(\Omega) \times L^\infty(\Omega) & \longrightarrow & L^2(\Omega)^2 \\ & (\lambda, \mu) & \longmapsto & u_{\lambda,\mu}, \end{array}$$

with $u_{\lambda,\mu}$ solution of (3), is differentiable on the same open set and its differential is everywhere a compact operator.

Proof: see appendix A.

Proposition 1 is a general result when both Lamé coefficients depend on the space variable. In our application, the Poisson coefficient ν is assumed to be constant, hence

the two Lamé coefficients are related by $\lambda = \dfrac{2\nu}{1-2\nu}\mu$. When the parameter is Young's modulus E, we have

$$\lambda(x) = \frac{\nu E(x)}{(1+\nu)(1-2\nu)}, \quad \mu(x) = \frac{E(x)}{2(1+\nu)}, \tag{5}$$

and the parameter-to-state map $L^\infty(\Omega) \to L^2(\Omega)^2$, $E \mapsto u_E$ has also a compact differential.

3. Inverse problem and inversion method

The discretized version of the direct problem (3) when the Lamé coefficients are given by (5) is:

$$A(E)u = b, \tag{6}$$

where $A(E)$ is the $N \times N$ stiffness matrix, $E \in \mathbf{R}^p$ is the discretized Young's modulus and $u \in \mathbf{R}^N$ is the displacement. The solution of this system is denoted u_E.

The solution u_E is partially known through an observation (in our case, it consists of taking the radial component of the displacement). Let $L : \mathbf{R}^N \to \mathbf{R}^n$ be the state-to-observation operator: the observed quantity is $u_{\text{mes}} = Lu \in \mathbf{R}^n$. The inverse problem is: find the parameter E so that $Lu_E = u_{\text{mes}}$. This inverse problem is ill-posed and when real data are measured, u_{mes} is perturbed by noise. The following regularized problem is solved: find the parameter $E \in \mathbf{R}^p$ that minimizes the functional

$$j(E) = \frac{1}{2}\left(||Lu_E - u_{\text{mes}}||^2 + \alpha||E||^2\right) = \frac{1}{2}\left(||F(E)||^2 + \alpha||E||^2\right), \tag{7}$$

where α is a Tikhonov regularization parameter and $F : \mathbf{R}^p \to \mathbf{R}^n$ is defined by

$$F(E) = Lu_E - u_{\text{mes}}. \tag{8}$$

The minimum E_* of the functional j satisfies: $Dj(E_*) = 0$, in other words: for all $h \in \mathbf{R}^p$, $(DF(E_*).h, F(E_*)) + \alpha(E_*, h) = 0$. Gauss-Newton method defines a sequence that converges to E_*: it starts from an initial guess E_0, and the iterations are defined by $E_{k+1} = E_k + d_k$, where d_k is the solution of

$$(DF(E_k)^T DF(E_k) + \alpha I)d_k = -DF(E_k)^T F(E_k) - \alpha E_k. \tag{9}$$

It follows from proposition 1 that the linear operator $DF^T DF$ is the discrete version of a compact operator (in other words, its eigenvalues tend rapidly towards zero). As a consequence, equation (9) can be numerically solved using the conjugate gradient algorithm, without preconditioning. It is proved in [3] that if the spectrum of a symmetric positive operator K is clustered around zero, with a few eigenvalues away from zero, then the conjugate gradient without preconditioning applied to the equation $Kx = y$ converges in a few iterations when the discrepancy principle is used as a stopping rule (an explicit upper bound on the number of iterations is given). To prove such a result, the residue after m iterations of conjugate gradient is interpreted as the image of x by $r_m(K^*K)$ for some polynomial r_m. A precise study of the optimality

conditions satisfied by r_m yields an upper bound on the number of iterations necessary to meet the discrepancy principle. It is important to note that the iterations have to be stopped early (according to the discrepancy principle), otherwise small eigenvalues shall interfere in the solution, and give important and rapidly oscillating parts (that are irrelevant and unwanted).

The resolution of (9) using the conjugate gradient does not require the computation of the whole Jacobian matrix $DF(E_k) = DF$, it suffices to be able to make the product of $DF^T DF + \alpha I$ by any given vector. The key now is to observe that, given a vector x, $DF^T DFx$ can be obtained using algorithmic differentiation rules [12]. We proceed as follows:

(i) **Computing** $z = DFx$
It is the directional derivative of a vectorial function, we use direct differentiation.

(ii) **Computing** $DF^T z$
It is a scalar criterion, we use reverse mode of algorithmic differentiation.

More precisely:

Proposition 2 (Computing $z = DFx$) *Let $x \in \mathbf{R}^p$ and let $z = DF(E)x$, then*

$$z = L\delta \tag{10}$$

where δ is solution to the linear system

$$A(E)\delta = -DA(E).x\, u_E. \tag{11}$$

Proof: Differentiating the relation $A(E)u_E = b$, it follows that for all $h \in \mathbf{R}^p$:

$$DA(E).h\, u_E + A(E)Du_E.h = 0. \tag{12}$$

Hence $DFx = L\, Du_E.x = L\delta$ with δ satisfying $A(E)\delta = -DA(E).x\, u_E$. □

Proposition 3 (Computing $DF^T z$) *Let $v_E \in \mathbf{R}^N$ be the adjoint state, that is v_E is the solution of the linear system*

$$A^T v = -L^T z. \tag{13}$$

Then for any vector $h \in \mathbf{R}^p$:

$$(DF^T z, h) = [D(F^T z)].h = (DA(E).h\, u_E, v_E) \tag{14}$$

Proof: Consider the Lagrangian operator:

$$\mathcal{L}(E, u, v) = (Lu - u_{\text{mes}}, z) + (A(E)u - b, v). \tag{15}$$

Then $F^T z = \mathcal{L}(E, u_E, v)$ hence

$$D_E(F^T z) = D_1\mathcal{L}(E, u_E, v) + D_2\mathcal{L}(E, u_E, v).D_E u_E.$$

Take $v = v_E$ satisfying $A^T v_E = -L^T z$ so that the second term above vanishes: it follows $D(F^T z).h = D_1\mathcal{L}(E, u_E, v_E).h = (DA(E).h\, u_E, v_E)$. □

Note: this result should be used with $h = e_i,\ 1 \le i \le p$ vector of the canonical basis of the discretized space, so as to obtain the components of the vector $DF^T z$. However we will see that the vector $DF^T z$ is evaluated in one single calculation provided the quantities ∇u_E and ∇v_E are available, since the quantity $(DF^T z, e_i)$ reduces then to an integration over one triangle of the mesh.

4. Numerical results

We modeled an experiment of elastography in a cross-section of a cylindrical gelatin phantom, as described in [14] and in section 5. Our numerical experiment is as follows: the domain Ω is an annulus between two concentric circles, centered at the origin. On the inner boundary we apply a Dirichlet condition consisting of radial displacement of constant norm. On the outer boundary we impose homogeneous Neumann condition, see figure 1(a). The Poisson coefficient $\nu = 0.45$ is constant over the whole domain, Young's modulus is constant (equal to 1) in all the domain, excepted in some inclusions (to be detected) where its value is 4 times higher, the value 4 is the contrast of the inclusion. The measured data u_{mes} is the radial component of the displacement at each point of the domain.

This problem was discretized using P1 finite elements, which are sufficient because we need only to evaluate the first order derivatives of the displacement. The algorithms described in appendix B have been implemented using `Matlab (The MathWorks, Inc.)` and the library `Getfem++ (www-gmm.insa-toulouse.fr/getfem/)` for finite element methods computations on a 1.6 GHz computer. The non-uniform triangular mesh has $p = 4108$ elements and $n = 2137$ points, and was generated using `emc2`.

We adopt the same notations for the discretized quantities as for the continuous ones: E denotes the Young's modulus distribution, u_E is the solution of the problem and the state-to-observation operator L is the linear operator consisting of taking the radial part of a vector field. F is defined by $F(E) = Lu_E - u_{\text{mes}}$. It follows from proposition 1 that the operator $E \mapsto u_E$ has a compact differential, hence $DF^T DF$ is also compact

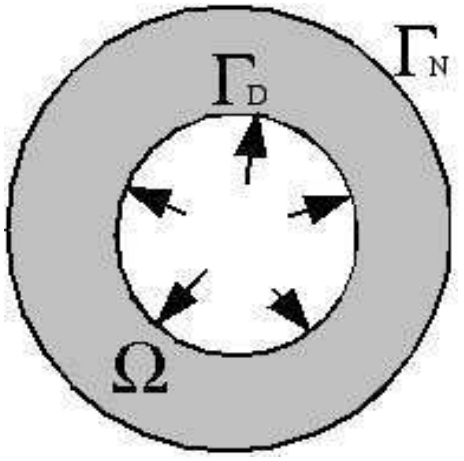

(a) The domain Ω, the Neumann boundary Γ_N, the Dirichlet boundary Γ_D (displacement indicated by arrows)

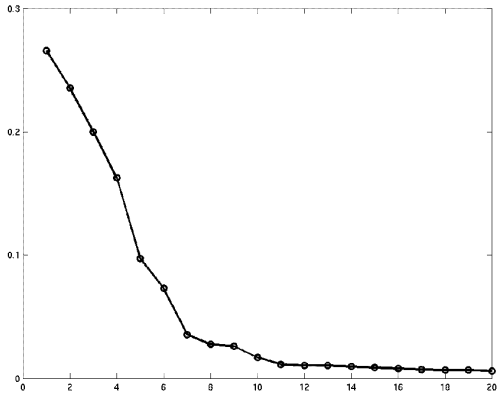

(b) The 20 largest eigenvalues of $DF^T DF$ (horizontal axis: number of eigenvalue ; vertical axis: eigenvalue)

Figure 1.

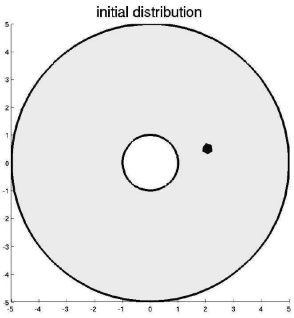

(a) True inclusion

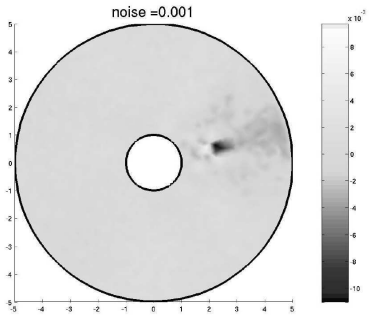

(b) Initial difference

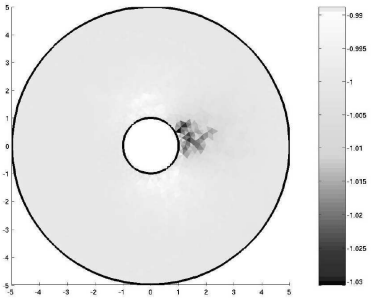

(c) the gradient method after 4 steps

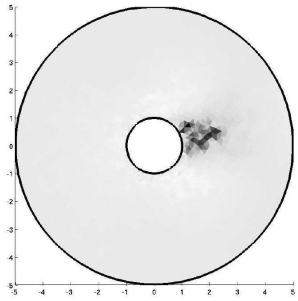

(d) the gradient method after 28 steps

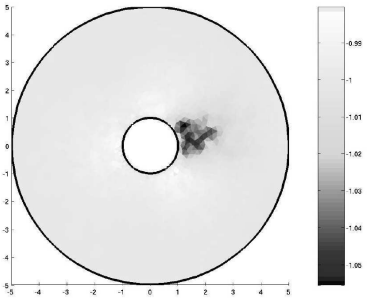

(e) First step of our method

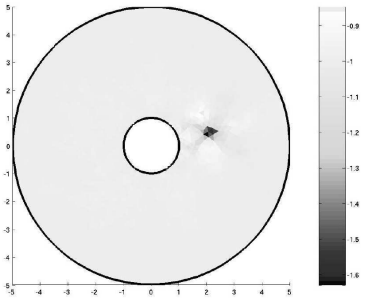

(f) Second step of our method

Figure 2. First set of results (0.1% noise). The color scale is reversed for the sake of visibility.

(this is illustrated on figure 1(b) where the 20 largest eigenvalues out of more than 4000 from the discretized version of DF^TDF are displayed).

Each conjugate gradient (CG) converged within a few iterations (see the last column in table 1), since the relative residue is set to 0.1, in accordance with the discrepancy

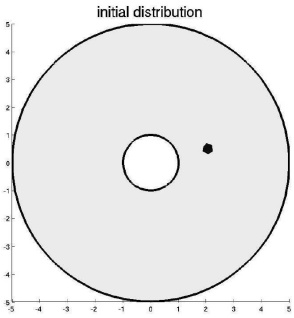

(a) True inclusion

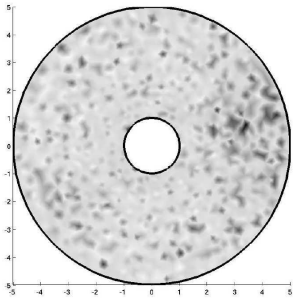

(b) Initial difference

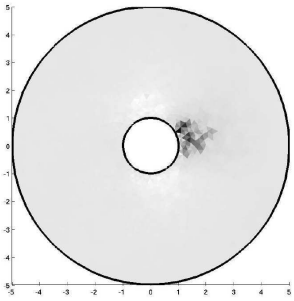

(c) the gradient method after 4 steps

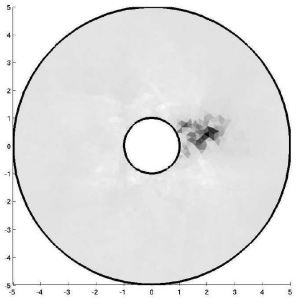

(d) the gradient method after 54 steps

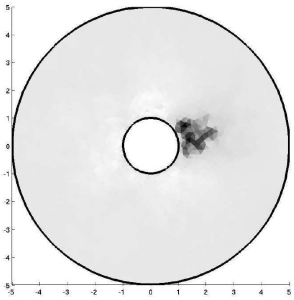

(e) First step of our method

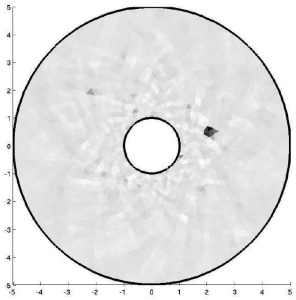

(f) Second step of our method

Figure 3. Second set of results (2% noise)

principle. The regularization parameter α is chosen once for all following the L-curve method [3].

We show one set of results for an almost noiseless reconstruction (0.1% uniformly-distributed noise) in figures 2(a)-2(f), and one set of results with 2% noise in figures 3(a)-3(f). We show a) Young's modulus distribution, b) the difference $Lu_0 - u_{\text{mes}}$, where

Table 1. Computation time and number of iterations of the gradient method (left) and our method (right), with 0.1% noise (top) and 2% noise (bottom).

First set of results, with 0.1% noise (figures 2(a)-2(f))			
gradient method		our method	
time (s)	total nb of iterations	time (s)	total nb of CG iterations
40.7	4 (=2×2)	60.1	2
249	28 (=2×14)	263.8	14
Second set of results, with 2% noise (figures 3(a)-3(f))			
gradient method		our method	
time (s)	total nb of iterations	time (s)	total nb of CG iterations
39.9	4 (=2×2)	60.6	2
501.1	54 (=2×27)	527.6	27

u_0 is the displacement when homogeneous distribution of Young's modulus is assumed, and the first iterations obtained c-d) by the gradient method, and e-f) by our method.

Our method is compared to the gradient method (named the adjoint method in [10], or steepest descent method). For this last method, at each step the value of Young's modulus is updated with $E_{k+1} = E_k + d_k$ where $d_k = -DF(E_k)^T F - \alpha E_k = -\nabla j(E_k)$. We show in table 1 the computation times for the results presented. It must be noted that when one iteration of Gauss-Newton algorithm is performed, several calls are made to algorithm 2 (this is when the conjugate gradient is used, since it is an iterative method): these are called CG iterations in table 1, and sub-iterations in [10]. During each sub-iteration, one direct and one adjoint problem are solved; on the other hand, when one step of the gradient method is performed, one adjoint problem is solved. Thus, in order to compare our method with the gradient method, we show the results of the gradient method after $2m$ iterations, where m is the number of sub-iterations in our method (so as to have solved the same total number of problems). Indeed, the computation times are of the same order. A qualitative observation is that our method gives a more accurate reconstruction of the zone.

The computational cost can also be compared with the cost required to compute the full Jacobian matrix in the standard Gauss-Newton method [8]: one adjoint problem is solved for each column of the matrix, in our case it would require more than 4000 resolutions (more than 2000 resolutions if the Jacobian is computed row by row). With our method the complete estimation of Young's modulus is performed with only 28 resolutions (14 direct and 14 adjoint) with the first set of data, and 54 resolutions with the second set of data.

5. Experimental results

In this section our objective was to demonstrate the feasibility of generating an image of the modulus contrast experimentally in a phantom. The experiment was designed to use an existing elastography system designed for prostate imaging and described in [14]. The ultrasonic probe was covered by a latex balloon filled with a coupling liquid that ensured good acoustic coupling between the probe and the phantom.

A hollow cylindrical phantom was prepared (see figure 4). It consisted in a homogeneous background material (gelatin, agar and water) into which six long, thin parallelepipedic samples of hydrophilic floral foam were inserted to create stiff inclusions of various thicknesses, ranging from 0.55mm to 2.6mm. The foam samples were beforehand soaked in degassed water in order to chase air bubbles that would otherwise hinder acoustic imaging. All foam samples were positioned at equal depth, spaced uniformly, with their long axis parallel to the axis of the cylinder. The imaging probe was inserted into the phantom and held stationary.

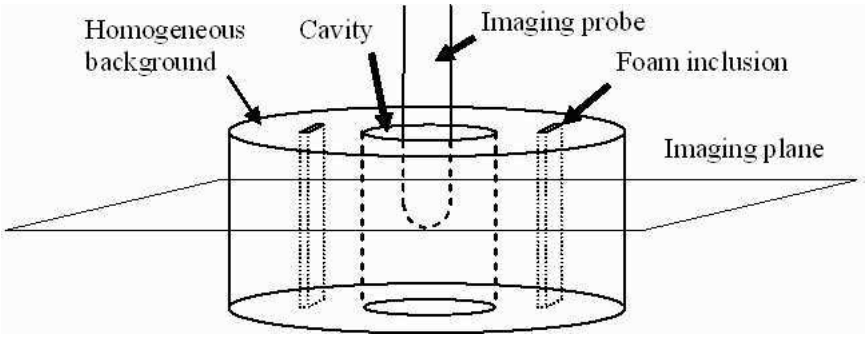

Figure 4. Experimental setup. The tip of the imaging probe is covered by a latex balloon that fills the whole cavity once it is inflated. For the sake of simplicity, only two (out of six) foam inclusions are shown.

The phantom was compressed by inflating the balloon. Data acquisition and displacement estimation was performed using a multi-compression sequence and a cross-correlation algorithm described in [15] (except for lateral motion estimation that was disabled). The radial strain is the derivative of the radial displacement along the radial lines. The maximum displacement was 1.7mm, the maximum strain approx.5% and the average strain 2.3%. The sonogram is shown on figure 5(a) and the strain elastogram is shown on figure 5(b). The reconstruction method explained above was applied to radial displacement data obtained from this experiment.

First step: identification of the background values

Since there are small inclusions in a homogeneous background, as a first approximation Young's modulus is assumed to be constant in the domain, equal to say E_0. The Poisson coefficient ν is also given a constant value ν_0.

The first task is to evaluate E_0 and ν_0. Let u_D^{mes} be the measured radial displacement on the Dirichlet boundary Γ_D. As a first approximation, the displacement is radial on

Γ_D and is equal to u_D^{mes}, and the boundary forces on Γ_N are zero. Under this assumption, the displacement inside the domain Ω does not depend on the value of E_0, it depends only on ν. We take $E_0 = 1$, and select by a one-dimensional search the value ν_0 of ν providing the smallest residue $||u_{\text{mes}} - Lu||$. In our case, we find $\nu_0 = 0.45$.

Second step: identification of the boundary conditions

As a second step, we identify the boundary conditions. In our experimental setup, it was not possible to impose the displacement precisely on the inner boundary. The outer boundary was left free, but the phantom was immersed in water, so pressure forces were present, moreover the phantom had to be maintained in order to prevent it from slipping away. This experiment was intended to be close from the clinical situation.

Knowing the background value of E_0 and ν_0, we address the following problem: as a direct problem, the boundary conditions g_N on Γ_N and u_D on Γ_D give rise to a unique solution $u(g_N, u_D)$ of the elastostatics problem. The inverse problem is: find the boundary conditions (g_N, u_D) so that the radial component $Lu(g_N, u_D)$ of the resulting state is close from u_{mes}. This inverse problem is solved with a Gauss-Newton algorithm similar to the one exposed above (it is simpler since the inverse problem is linear), a H^1-semi-norm Tikhonov regularization term is added. As initial guess, it is natural to take $g_N = 0$ and u_D equal to the measured radial displacement. We show the residues $Lu(g_N, u_D) - u_{\text{mes}}$ at the initial guess in figure 6(a) and after 4 Gauss-Newton steps in figure 6(b). Indeed, "butterfly wings" patterns can be seen around the 4 main inclusions. This is an a-posteriori justification of all the approximations made above.

Note that a different choice for E_0 would only have changed the value of the forces on the Neumann boundary by a constant factor: the choice of E_0 is a choice of unit for measuring the forces on the Neumann boundary, or equivalently a choice of unit for measuring Young's modulus. We only want to find a contrast of Young's modulus, that

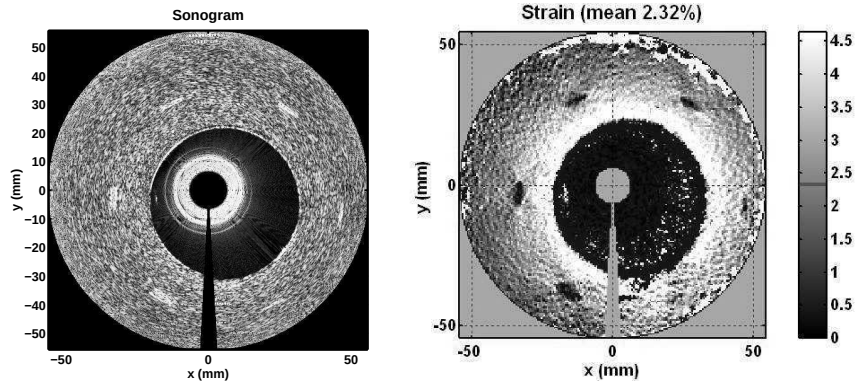

(a) (b)

Figure 5. (a) Sonogram, (b) strain elastogram with experimental data. The images correspond to a 55×55mm area. The thickest inclusion is located at 7:00 in the images, and the other inclusions are positioned clockwise by order of decreasing thickness.

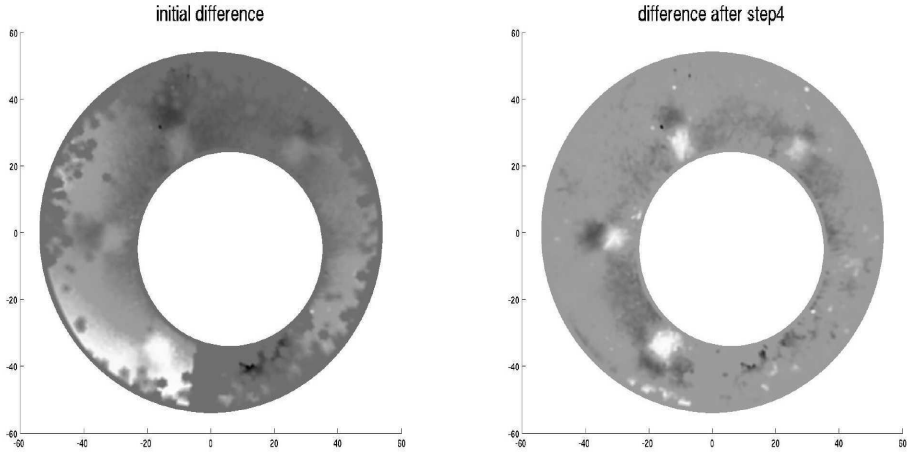

(a) (b)

Figure 6. The difference $Lu(g_N, u_D) - u_{\text{mes}}$ (a) at the initial guess, and (b) after 4 Gauss-Newton steps (computation time ≤ 1 minute).

is a ratio, hence the choice of the unit does not matter.

Third step: estimating Young's modulus contrast

The boundary conditions have been estimated. We apply then the algorithms of appendix B. The corresponding modulus contrast elastogram is shown in figures 7(a) and 7(b) with two different meshes. On the fine mesh, we suppress points where the data are too noisy, this is done using an additional data: the measure of correlation that is a natural data in elastography (it is the correlation between the signals before and after compression: when it is much smaller than 1, the measure is considered as not reliable). Among the six inclusions designed to test detectability, only the 4 largest ($\geq$ 1.3mm thick) were visible in the modulus reconstruction while 5 ($\geq$ 0.95mm) were visible in the strain elastogram, see figure 5(b). The thinest inclusion (0.55mm) was barely visible, even in the sonogram. This shows the power and the limitations of our method. No independent measurements are available for the true value of the contrast of the inclusion. Our future work will include independent quantitative measurement of the contrasts.

Conclusion

We presented here a general method for solving inverse problems. This method involves a zero memory Gauss-Newton algorithm using both direct and adjoint differentiation, and appears to be qualitatively more efficient than the gradient method. It was applied to the problem of recovering Young's modulus contrast of inclusions in an elastic medium from the measurements of one component of the displacement. It was validated both on numerical and experimental data. When applied to real data, our method also allowed

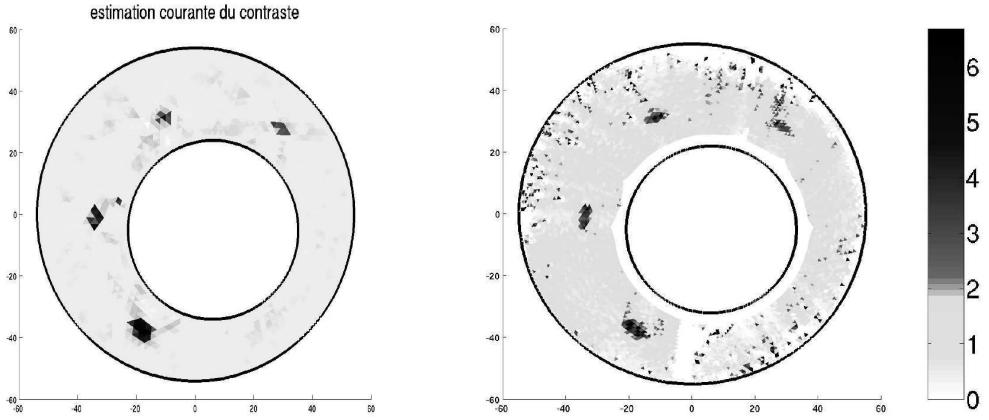

(a) (b)

Figure 7. Modulus contrast reconstruction with experimental data.
(a) on a mesh with ∼1600 nodes and ∼3000 triangles, reconstruction time ≤20 minutes
(b) on a finer mesh with ∼6000 nodes and ∼12000 triangles (in white: non reliable data), reconstruction time ≤2 hours

to estimate boundary forces (up to a multiplicative factor) when available data were only radial displacement measurements.

Acknowledgments

This work was supported in part by the National Cancer Institute (USA) Program Project Grant P01-64597 to the University of Texas in Houston ; and in part by ACINIM-IMEG CNRS Project (France).

Appendix A: proof of proposition 1

We give here the proof of proposition 1 (see [16] for an analysis in the dynamic case).

The following facts will be useful:

1) if (λ, μ) satisfies uniform coercivity, then the bilinear form $a_{\lambda,\mu}$ is coercive on $\mathcal{V}$:

$$a_{\lambda,\mu}(u,u) = \int_\Omega \sigma_{\lambda,\mu}(u) : \epsilon(u) \geq c||\epsilon(u)||^2_{L^2} \geq c'||u||^2_{H^1}, \tag{16}$$

where the last inequality follows from Korn's inequality.

2) the following inequality follows from Cauchy-Schwartz inequality: for all $u, v \in \mathcal{V}$,

$$|a_{\lambda,\mu}(u,v)| \leq 2(||\lambda||_\infty + ||\mu||_\infty)||\epsilon(u)||_{L^2}||\epsilon(v)||_{L^2}. \tag{17}$$

Step 1: Let us prove first that R is continuous. Consider $(\lambda_1, \mu_1) \in L^\infty(\Omega) \times L^\infty(\Omega)$ a value of the parameter satisfying the uniform coercivity and let $(\lambda_2, \mu_2) = (\lambda_1 + \delta, \mu_1 + \zeta)$ where (δ, ζ) lies in a small neighborhood $\mathcal{N}$ of the origin such that a constant c of uniform

coercivity holds for all (λ_2, μ_2) when $(\delta, \zeta) \in \mathcal{N}$. Let u_1 and u_2 be the associated solutions:

$$\forall v \in \mathcal{V}, \quad a_{\lambda_1,\mu_1}(u_1, v) = \ell(v), \tag{18}$$

$$\forall v \in \mathcal{V}, \quad a_{\lambda_2,\mu_2}(u_2, v) = \ell(v). \tag{19}$$

Note that $c||u_2||^2_{H^1} \leq |a_{\lambda_2,\mu_2}(u_2, u_2)| = |\ell(u_2)| \leq |||\ell|||.||u_2||_{H^1}$, hence $||u_2||_{H^1}$ remains bounded when $(\delta, \zeta) \in \mathcal{N}$. The difference $u_3 = u_2 - u_1$ satisfies:

$$\forall v \in \mathcal{V}, \quad a_{\lambda_1,\mu_1}(u_3, v) = -a_{\delta,\zeta}(u_2, v). \tag{20}$$

It follows from (20) with $v = u_3$, coercivity of a_{λ_1,μ_1} and (17) that:

$$c'||u_3||^2_{H^1} \leq |a_{\delta,\zeta}(u_2, u_3)| \leq 2(||\delta||_\infty + ||\zeta||_\infty)||\epsilon(u_2)||_{L^2}||\epsilon(u_3)||_{L^2} \tag{21}$$

from which the continuity of R follows, since $||\epsilon(u_3)||_{L^2} \leq ||u_3||_{H^1}$.

Step 2: Let us prove now that R is differentiable. Let (λ_1, μ_1) and (λ_2, μ_2) be as above. Let $d = d(\delta, \zeta) \in \mathcal{V}$ be the solution of

$$\forall v \in \mathcal{V} \quad a_{\lambda_1,\mu_1}(d, v) = -a_{\delta,\zeta}(u_1, v). \tag{22}$$

We now will prove

$$u_2 = u_1 + d(\delta, \zeta) + o_{H^1}(||(\delta, \zeta)||_\infty). \tag{23}$$

To check (23), note that the difference $r = u_2 - u_1 - d$ satisfies:

$$\forall v \in \mathcal{V}, \quad a_{\lambda_1,\mu_1}(r, v) = a_{\delta,\zeta}(u_2 - u_1, v). \tag{24}$$

Write (24) with $v = r$, use coercivity of a_{λ_1,μ_1} and (17) to obtain:

$$c'||r||^2_{H^1} \leq |a_{\delta,\zeta}(u_2 - u_1, r)| \leq 2(||\delta||_\infty + ||\zeta||_\infty)||\epsilon(u_2 - u_1)||_{L^2}||\epsilon(r)||_{L^2}. \tag{25}$$

Since $||\epsilon(u_2 - u_1)||_{L^2}$ tends to zero as (δ, ζ) tends to zero and $||\epsilon(r)||_{L^2} \leq ||r||_{H^1}$, it follows that $r = o_{H^1}(||(\delta, \zeta)||_\infty)$ which proves (23). It is clear that the map $(\delta, \zeta) \mapsto d(\delta, \zeta)$ is linear continuous, hence it is the differential of the parameter-to-state map R.

Step 3: The second part of the proposition follows from the first part and the fact that the embedding $H^1(\Omega) \hookrightarrow L^2(\Omega)$ is compact. □

Appendix B: the algorithms

Algorithm 1: Finding the Young's modulus distribution (k-th step of Gauss-Newton method)

input : *mesh, Young's modulus distribution* $E = E_k$, ν, *boundary conditions,* u_{mes}, *regularization parameter* α
- compute the stiffness matrix $A(E)$, compute the direct state u_E,
- construct the matrix L from mesh data,
- compute the adjoint state v_E,
- compute DF^TF using the formula given in Proposition 3.
- find the solution d of $(DF^TDF + \alpha I)d = -DF^TF - \alpha E$ using the conjugate gradient, the multiplication of a vector by DF^TDF is given by algorithm 2
- the estimated Young's modulus distribution is $E_{k+1} = E_k + d$.

Algorithm 2: Computing $y = DF^T DFx$ for a given vector x

input : *vector x, mesh, ν, stiffness matrix $A(E)$, direct state u_E, matrix L*
- compute $\delta = -A(E)^{-1}[A(x) - A(0)]u_E$,
- compute $z = L\delta$: we have $z = DFx$,
- compute the adjoint state v_E solution of $A^T v = -L^T z$,
- compute $\sigma(u_E)$ and $\epsilon(v_E)$,
- the coordinates (y_i) of y in the canonical basis are given by

$$(*) \quad y_i = \int \sigma(u_E) : \epsilon(v_E)$$

where the integral is taken over the triangle with label i.

justification of $(*)$: if K is a stiffness matrix and (ϕ^i) is the base of the space of functions, then

$$K_{i,j} = \int_\Omega \sigma(\phi^i) : \epsilon(\phi^j)\, dx, \tag{26}$$

hence $(Ku_E, v_E) = \int_\Omega \sigma(u_E) : \epsilon(v_E)\, dx$ which reduces to an integral over one triangle if $K = A(e_i)$ is an elementary stiffness matrix.

References

[1] Ophir J, Cespedes I, Ponnekanti H, Yazdi Y and Li X 1991 *Elastography: a quantitative method for imaging the elasticity of biological tissues*, Ultrasonic imaging **13**, 111–134

[2] Ophir J, Alam S, Garra B, Kallel F, Konofagou E, Krouskop T, Merritt C, Righetti R, Souchon R, Srinivasan S and Varghese T 2002 *Elastography: Imaging the Elastic Properties of Soft Tissues with Ultrasound*, J Med Ultrasonics **29**, 155–171

[3] Engl H, Hanke M and Neubauer A 2000 *Regularization of Inverse Problems*, Kluwer Academic Publishers

[4] Dennis J and Schnabel R 1996 *Numerical methods for Unconstrained Optimization and Nonlinear Equations*, Classics in Appl.Math.Sc, SIAM

[5] Kirsch A 1996 *An introduction to the mathematical theory of inverse problems*, Springer

[6] Kallel F and Bertrand M 1996 *Tissue elasticity reconstruction using linear perturbation method*, IEEE Transactions on Medical Imaging **15**(3), 299–313

[7] Doyley M, Meaney P and Bamber J 2000 *Evaluation of an iterative reconstruction method for quantitative elastography*, Physics in Medicine and Biology **45**, 1521–1540

[8] Doyley M, Srinivasan S, Pendergrass SA, Wu Z and Ophir J 2005 *Comparative evaluation of strain-based and model-based modulus elastography*, Ultrasound Med. Biol. **31**(6), 787–802

[9] Le Dimet FX and Talagrand O 1986 *Variational Assimilation of Meteorological Observations: Theoretical aspect*, Tellus **38A**, 97–110

[10] Oberai A, Gokhale N and Feijóo G 2003 *Solution of inverse problems in elasticity imaging using the adjoint method*, Inverse Problems **19**, 297–313

[11] Oberai A, Gokhale N, Doyley M and Bamber J 2004 *Evaluation of the adjoint equation based algorithm for elasticity imaging*, Physics in Medicine and Biology **49**, 2955–2974

[12] Griewank A 2000 *Evaluating derivatives, Principles and Techniques of Algorithmic Differentiation*, Frontiers in Applied Mathematics, SIAM

[13] Duvaut G and Lions JL 1972 *Les inéquations en mécanique et en physique*, Dunod

[14] Souchon R, Soualmi O, Bertrand M, Chapelon JY, Kallel F and Ophir J 2002 *Ultrasonic elastography using sector scan imaging and a radial compression* Ultrasonics **40**(1-8) 867–871

[15] Souchon R, Rouvière O, Gelet A, Detti V, Srinivasan S, Ophir J and Chapelon JY 2003 *Visualisation of HIFU lesions using elastography of the human prostate in vivo* Ultrasound Med.Biol. **29**(7) 1007–1015

[16] Chi DP and Kim J 2000 *Parameter estimation of elastic media*, in Inverse problems and related topics, Nakamura *et al.* ed., Research Notes in Mathematics **419**, Chapmann & Hall, 37–55